ORIGINAL PAPER

Distinguishing features of microglia- and monocyte-derived macrophages after stroke

Golo Kronenberg[1,2,3] · Ria Uhlemann[1] · Nadine Richter[4] · Friederike Klempin[1,2,4] · Stephanie Wegner[1] · Lilian Staerck[4] · Susanne Wolf[4] · Wolfgang Uckert[4,5] · Helmut Kettenmann[4] · Matthias Endres[1,6] · Karen Gertz[1]

Abstract

After stroke, macrophages in the ischemic brain may be derived from either resident microglia or infiltrating monocytes. Using bone marrow (BM)-chimerism and dual-reporter transgenic fate mapping, we here set out to delimit the responses of either cell type to mild brain ischemia in a mouse model of 30 min transient middle cerebral artery occlusion (MCAo). A discriminatory analysis of gene expression at 7 days post-event yielded 472 transcripts predominantly or exclusively expressed in blood-derived macrophages as well as 970 transcripts for microglia. The differentially regulated genes were further collated with oligodendrocyte, astrocyte, and neuron transcriptomes, resulting in a dataset of microglia- and monocyte-specific genes in the ischemic brain. Functional categories significantly enriched in monocytes included migration, proliferation, and calcium signaling, indicative of strong activation. Whole-cell patch-clamp analysis further confirmed this highly activated state by demonstrating delayed outward K^+ currents selectively in invading cells. Although both cell types displayed a mixture of known phenotypes pointing to the significance of 'intermediate states' in vivo, blood-derived macrophages were generally more skewed toward an M2 neuroprotective phenotype. Finally, we found that decreased engraftment of blood-borne cells in the ischemic brain of chimeras reconstituted with BM from $Selplg^{-/-}$ mice resulted in increased lesions at 7 days and worse post-stroke sensorimotor performance. In aggregate, our study establishes crucial differences in activation state between resident microglia and invading macrophages after stroke and identifies unique genomic signatures for either cell type.

Keywords Cerebral ischemia · Bone-marrow chimera · Microglia · Macrophage · Middle cerebral artery occlusion

Introduction

In health, microglia self-maintain independent of hematopoietic stem cells (HSCs) and there is practically no background trafficking of blood-derived cells into the adult brain parenchyma [1, 17, 56, 58, 64]. It is only after significant injury that

Matthias Endres and Karen Gertz contributed equally.

Electronic supplementary material The online version of this article (https://doi.org/10.1007/s00401-017-1795-6) contains supplementary material, which is available to authorized users.

✉ Karen Gertz
karen.gertz@charite.de

1 Center for Stroke Research, Klinik für Neurologie, and Department of Experimental Neurology, Charité – Universitätsmedizin Berlin, corporate member of Freie Universität Berlin, Humboldt-Universität zu Berlin, and Berlin Institute of Health, Charitéplatz 1, 10117 Berlin, Germany

2 Klinik für Psychiatrie und Psychotherapie, Campus Mitte, Charité-Universitätsmedizin Berlin, corporate member of Freie Universität Berlin, Humboldt-Universität zu Berlin, and Berlin Institute of Health, Charitéplatz 1, 10117 Berlin, Germany

3 Klinik und Poliklinik für Psychiatrie und Psychotherapie, Zentrum für Nervenheilkunde, Universitätsmedizin Rostock, Gehlsheimer Straße 20, 18147 Rostock, Germany

4 Max-Delbruck-Center for Molecular Medicine (MDC) in the Helmholtz Association, Robert-Roessle-Str. 10, 13125 Berlin, Germany

5 Institut für Biologie, Humboldt-Universität Berlin, Robert-Roessle-Str. 10, 13125 Berlin, Germany

6 DZNE (German Center for Neurodegenerative Diseases), Charitéplatz 1, 10117 Berlin, Germany

monocytes enter the brain. Both cell types may produce macrophages in CNS pathologies that are virtually impossible to distinguish based on morphological criteria alone [10, 39, 52, 55]. However, microglia and monocytes differ in their ancestry. At an early time in ontogeny, progenitors in the embryonic yolk sac give rise to microglia-like cells in the brain rudiment which then expand dramatically with only marginal replacement by HSC-derived progenitors [2, 21]. By contrast, postnatal monocytes continuously form from HSCs, which, unlike the progenitors of microglia, depend on the MYB family of transcription factors [4, 22].

Due to its protracted time course, post-stroke inflammation may be an attractive target for new therapies. Neuroinflammation is an important, yet still somewhat poorly defined, element in the pathogenesis of ischemic stroke which may entail both propitious and detrimental consequences [15, 54]. Microglia as well as monocyte-derived macrophages populate the infarct [70] and show enhanced phagocytic activity [59]. Moreover, these two cell types typically display electrophysiological features of stimulated, cultured microglia after stroke [31, 37]. Exciting recent research is beginning to specifically uncover how hematogenous macrophages re-establish the blood–brain barrier, infiltrate the brain in a CCR2-dependent fashion, and contribute to repair of the ischemic neurovascular unit [18, 19].

Here, we performed dual-reporter experiments and traced the influx of DsRed-transduced blood-borne macrophages into the ischemic brain after 30 min middle cerebral artery occlusion (MCAo)/reperfusion. Chimeric mice harboring resident microglia expressing EGFP (i.e., macrophage colony-stimulating factor 1 receptor-EGFP transgenic mouse model; [61, 62]) were employed. This combined approach not only permits convenient detection of microglia and invaded macrophages for further histological and detailed physiological analyses, but also greatly facilitates isolation of these cells from the brain for transcriptional profiling. In a next step, to further dissect how blood-borne cells impact stroke outcome, we performed additional experiments in BM chimeric mice with donor BM lacking P-selectin glycoprotein ligand-1 (PSGL-1, encoded by the gene *Selplg*), a crucial factor in leukocyte recruitment into inflamed tissue [60, 65]. Our results establish meaningful differences between microglia and invaded monocytes after brain ischemia and demonstrate beneficial effects of the latter on the pathogenesis of stroke.

Methods

Mice

All experimental procedures were approved by the necessary official committees and carried out in accordance with the Animal Welfare Act, the European Communities Council Directive of November 24, 1986 (86/609/EEC) and the ARRIVE guidelines [33]. The generation and characterization of colony-stimulating factor-1 receptor (CSF1r)-EGFP transgenic mice has been reported previously ('MacGreen' mice [61, 62]). P-selectin glycoprotein ligand (PSGL)-1-deficient mice (Selplg-KO mice) have been described earlier [78]. Male wild-type C57BL/6J and Selplg-KO mice were from the Jackson Laboratory (Bar Harbor, ME). At the beginning of experiments, animals were 8–10 weeks old and weighed 18–22 g. Mice were group housed with ad libitum access to food and water.

Generation of bone marrow (BM) chimeric mice

BM chimeras were generated as described [15, 24, 67]. Single cell bone marrow (BM) suspension was prepared from hind leg tibias and femurs of donor mice. BM cells were enriched for HSCs using the EasySep mouse SCA1-positive selection kit (#18756, StemCell Technologies) according to the manufacturer's protocol. These cells were then prestimulated at a density of 10^6/ml for 3 days in StemPro-34 serum-free medium (#10639-001 Invitrogen) supplemented with 5% FCS (#1502-P111504, PAN Biotech), 100 U/ml penicillin/streptomycin (#A2212, Biochrome), 2 mM L-glutamine (#K0282, Biochrome), 10 ng/ml murine IL-3 (#213-13, Peprotech), 50 ng/ml murine interleukin-6 (IL-6) (#216-16, Peprotech), and 50 ng/ml murine stem cell factor (#250-03, Peprotech). 24-well non-tissue culture plates (Becton–Dickinson, Heidelberg, Germany) were coated with 20 µg/ml RetroNectin (#T100A/B, TaKaRa) according to the manufacturer's instructions. On day 3, plates were loaded with 500 µl virus supernatant per well and centrifuged for 90 min at $2500 \times g$ and 4 °C. EGFP- or DsRed-bearing retroviruses were described previously [74]. After equilibration to ambient temperature, virus supernatant was aspirated and target cells, adjusted to 4×10^5/ml in freshly supplemented media, were disseminated. Cells were cultured overnight in these RetroNectin/virus-coated plates. Retroviral transduction was repeated on day 4. One day later, BM cells were harvested and 1×10^6 cells were i.v. injected into recipient mice which had received lethal whole-body irradiation (950 rad) to suppress endogenous hematopoiesis. Recipient mice received drinking water supplemented with fluoroquinolone antibiotic enrofloxacin (0.01% Baytril®, Bayer Vital) for 5 weeks.

Induction of cerebral ischemia

Mice were anesthetized for induction with 1.5% isoflurane and maintained in 1.0% isoflurane in 69% N_2O and 30% O_2 using a vaporizer. Left middle cerebral artery occlusion (MCAo) was essentially performed as described elsewhere [12]. In brief, brain ischemia was induced with an 8.0 nylon monofilament coated with a silicone resin/hardener mixture

(Xantopren M Mucosa and Activator NF Optosil Xantopren, Haereus Kulzer, Germany). The filament was introduced into the internal carotid artery up to the anterior cerebral artery. Thereby, the middle cerebral artery and anterior choroidal arteries were occluded. The filament was removed after 30 min to allow reperfusion.

Cell isolation and flow cytometry

Blood was collected in plasma tubes (Microvette® 500K3E, Sarstedt, Germany). Within 30 min, blood was transferred into polystyrene tubes (VWR, Darmstadt, Germany) and incubated with rat anti-mouse CD16/CD32 antibodies (clone 2.4G2; 1:200; BD Biosciences) for 5 min at 4 °C. Cells were stained for 15 min. Red blood cells were lysed with BD Pharm Lyse (BD Biosciences) according to the manufacturer's instructions.

On day 7 after 30 min MCAo/reperfusion, brains of MacGreen mice were removed. A 4-mm coronal section was quickly dissected from the left (i.e., ischemic) hemisphere (approximately + 5.8 to 1.8 mm from interaural line) and homogenized. CD11b$^+$ cells were enriched from the ischemic brain using a MACS protocol combined with prior myelin removal (Miltenyi Biotec, Bergisch Gladbach, Germany). Positively selected CD11b$^+$ cells were incubated with 10 μg/ml propidium iodide to stain for non-living cells. Cells were sorted on a FACSAria II (BD Biosciences, Heidelberg, Germany). Cells stained for CD11b could be easily subdivided into two distinct subsets: CD11b$^+$ EGFP$^+$ PI$^-$ microglia and CD11b$^+$ DsRed$^+$ PI$^-$ invading monocytes. To eliminate debris and doublets, a sequential gating strategy based on SSC-H/SSC-W and FSC-H/FSC-W was employed. The entire gating strategy is outlined in Fig. 3c. The resultant samples were subsequently used for transcriptomic analysis (see below). In a separate, more sophisticated, FACS experiment, CD11b$^+$ cells were further analyzed for key markers of different types of immune cell. The following antibodies were used (all from BD Biosciences): CD3 V450, clone 500A2, 1:100; CD45 V500, clone 104, 1:100; CD19 PerCP-Cy™5.5, clone 1D3, 1:800; Ly6C PE-Cy™7, clone AL-21, 1:800; Ly6G APC-Cy™7, clone 1A8, 1:100; CD11b APC, clone M1/70, 1:100; CD335 (NKp46) PerCP-Cy™5.5, clone 29A1.4, 1:100. Samples were acquired on a flow cytometer (BD FACSCantoTM II). Data were analyzed with the FlowJo software v10 (Tree Star; Ashland, OR, USA).

Gene expression

Total RNA was extracted from FACS-sorted cells using the NucleoSpin® RNA extraction kit (Macherey–Nagel). RNA samples were quality checked via the Agilent 2100 Bioanalyzer platform and using the Agilent 2100 Bioanalyzer expert

software (Agilent Technologies). Gel images, electropherograms and RIN numbers confirmed high RNA quality of all samples. Subsequently, SuperAmp RNA amplification (Miltenyi Biotec) was performed. Briefly, the amplification is based on a global PCR protocol using mRNA-derived cDNA. mRNA was isolated via magnetic bead technology. After SuperAmp® RNA amplification, the integrity of cDNA was again checked with the Agilent 2100 Bioanalyzer platform (AgilentTechnologies). The average length of the highly amplified cDNA products ranged between 200 and 1000 base pairs. 250 ng of each of the cDNAs were used as template for Cy3 labeling. The Cy3-labeled cDNAs were hybridized overnight (17 h, 65 °C) to Agilent Whole Mouse Genome Oligo Microarrays 8 × 60 K. Fluorescence signals of the hybridized Agilent Microarrays were detected using Agilent's Microarray Scanner System (Agilent Technologies). Detailed information on the microarray experiments reported here including all data sets was submitted to NCBI's Gene Expression Omnibus (GEO) [11], and are accessible through GEO Series accession number GSE64811.

Data preprocessing

The background-corrected intensity data of all individual microarrays included in the analysis were compiled in one file. After background correction, quantile normalization was conducted between arrays. The normalized intensities were then log2-transformed and served as the basis for further analyses.

Selection of differentially expressed genes

Normalized intensity data were compared with Student's t test with paired design to determine differences in gene expression between the two sample groups. For these comparisons, an unadjusted p value ≤ 0.05 was used. In addition, the difference in the median expression values between the sample groups was computed. Candidate genes were required to show expression differences of at least fourfold (i.e., log2 ratio $\leq - 2$ or ≥ 2). The selected candidate genes were additionally filtered to allow only up to one flagged sample in the group with higher expression (Rosetta Resolver error model [76]).

Functional grouping analysis and annotation enrichment analysis

A functional grouping analysis was conducted to gain an overview of the different biological processes associated with the identified candidate genes. The annotations used were derived from Gene Ontology (GO), which provides information on molecular function, as well as from various pathway resources for information on involvement in

biological signaling pathways. All annotations were summarized and curated by the Miltenyi Bioinformatics team. For an assessment of the true enrichment of a category, Fisher's exact test with Benjamini–Hochberg correction for multiple testing was performed. Moreover, the two sets of candidate reporters were subjected to a manually curated biological pathway analysis. In brief, the differentially expressed reporters were tested for significant enrichments of annotations using the TreeRanker software (Miltenyi Biotec) as described recently [72].

Histochemistry and immunohistochemistry

After a lethal overdose of anesthetics, animals were transcardially perfused with physiological saline followed by 4% PFA in 0.1 M phosphate buffer, pH 7.4. Brains were dissected from the skulls and postfixed overnight. Before sectioning from a dry ice-cooled copper block on a sliding microtome (Leica), the brains were transferred to 30% sucrose in 0.1 M phosphate buffer, pH 7.4, until they sank. Brains were cut in the coronal plane into 40-μm-thick sections. Sections were stored at − 20 °C in cryoprotectant solution (25% ethylene glycol, 25% glycerol, and 0.05 M phosphate buffer). Sections were stained using free-floating immunohistochemistry. Primary antibodies were applied in the following concentrations: anti-DsRed (goat, 1:100, Santa Cruz, Dallas, TX, #sc-33353), anti-GFP (chicken, 1:200, Limerick, Rockland, PA, #600-901-215), anti-Iba1 (rabbit, 1:500, Wako, Neuss, Germany, #019-19741), and anti-NeuN (mouse, 1:100, Chemicon, Temecula, CA, #MAB377). Immunohistochemistry followed the peroxidase method with biotinylated secondary antibodies (all: 1:500; Jackson ImmunoResearch Laboratories, West Grove, PA), ABC Elite reagent (Vector Laboratories, Burlingame, CA) and diaminobenzidine (DAB; Sigma) as chromogen. For immunofluorescence FITC- (#703-095-155), RhodX- (#705-295-147) or Alexa Fluor 647- (#711-605-152) conjugated secondary antibodies (all from Dianova) were all used at a concentration of 1:125. Fluorescent sections were coverslipped in polyvinyl alcohol with diazabicyclooctane (DABCO) as anti-fading agent.

Quantification and imaging

Lesion volume was measured as described earlier [80]. Similarly, the number of cells per volume was assessed using StereoInvestigator® software (MicroBrightfield, Colchester, VT) as described previously [16]. Briefly, in defined reference sections (i.e., interaural + 5.34, + 3.94 and + 1.86 mm) the ischemic lesion was delineated at 100× magnification and EGFP+ invaded cells were counted at 200× magnification. Confocal microscopy was performed using a spectral confocal microscope (Zeiss, LSM 700). Appropriate gain and black level settings were determined on control slices stained with secondary antibodies alone.

Magnetic resonance imaging (MRI)

MRI was performed using a 7 Tesla rodent scanner (Pharmascan 70/16, Bruker BioSpin, Ettlingen, Germany) and a 20-mm-^{1}H-RF quadrature-volume resonator. A T2-weighted 2D turbo spin-echo sequence was used (imaging parameters TR/TE = 4200/36 ms, rare factor 8, 4 averages, 32 axial slices with a slice thickness of 0.5 mm, field of view of 2.56 × 2.56 cm, matrix size 256 × 256). Lesion volume was quantified with Analyze 10.0 (AnalyzeDirect, Inc.; Lenexa, KS).

Tissue preparation for electrophysiology

Acute coronal brain slices of 150 μm thickness were prepared as described [25]. Mice were decapitated, the cranium was opened, and the brain was carefully removed. Brain stem and cerebellum were removed from the cerebrum. Then the cerebrum was fixed with conventional superglue on a metal disc in the vibratome chamber (Microm HM 650, Microm International GmbH, Waldorf, Germany). Slice preparations were carried out in ice-cold bicarbonate-buffered artificial cerebrospinal fluid (ACSF: 134 mM NaCl, 2.6 mM KCl, 1.3 mM MgCl$_2$, 2 mM CaCl$_2$, 1.25 mM K$_2$HPO$_4$, 10 mM C$_6$H$_{12}$O$_6$, 26 mM NaHCO$_6$, pH 7.4, osmolarity 340 mmol/kg). Subsequently, the brain slices were transferred into continuously gassed (95% O$_2$, 5% CO$_2$) ACSF at room temperature for approximately 30 min before conducting the experiments.

Patch-clamp recordings

Whole-cell patch-clamp recordings were performed 7–9 days after 30 min MCAo/reperfusion using an EPC 10 patch-clamp amplifier combined with the TIDA 5.24 software (Lambrecht, Germany). Acute brain slices were transferred into the holding chamber mounted on an upright microscope and superfused with ACSF at room temperature. Cells were visualized with a 60 × objective (Zeiss Axioskop 2 FS plus, Zeiss, Oberkochen, Germany). Patch pipettes were pulled with a Sutter Instrument Pipette Puller (HEKA Elektronik) from borosilicate capillaries and filled with standard intracellular solution (4 mM NaCl, 120 mM KCl, 4 mM MgCl$_2$, 0.5 mM CaCl$_2$, 10 mM Hepes, 5 mM EGTA, 5 mM glucose; pH 7.4). To confirm intracellular access, Alexa Fluor ® 594 was added to the pipette solution. For fluorescence imaging, EGFP or DsRed and Alexa594 were excited at 488 or 584 nm, and emitted light was measured at 530 ± 10 nm or 607 nm, respectively. Membrane currents were recorded with a series of voltage steps (10 mV

increment, filtered with 2.9 kHz) from a holding potential of -70 mV ranging from -150 to $+50$ mV for 50 ms. Capacitative transients were compensated by TIDA 5.24 software.

Sensorimotor outcome

To assess general fitness and motor coordination, animals were tested on the rotarod (TSE Sytems, Bad Homburg, Germany) and on the pole test at 72 and 96 h after MCAo/reperfusion, respectively. For the rotarod task, mice were placed on an accelerating rotating rod (acceleration from 2 to 40 rpm within 5 min) and a stop-clock was started. When the mice dropped and touched the sensing platform below, the stop-clock stopped automatically. Each animal performed three trials. The pole test was performed as described in detail previously [28]. A vertical steel pole was covered with tape (Durapore) to create a rough surface. The animal was placed head upward near the top of the pole. The time required to turn completely downward (t turn) and the total time to reach the floor with all four paws (t floor) were recorded. If the mouse was unable to turn completely, the time to reach the floor was also attributed to t turn. Each animal was tested on five trials and the average score was taken as the final pole test score.

Statistical analysis

Experiments were carried out in a blinded fashion. Data are presented as means $\pm$ SEM. Unless otherwise indicated, groups were compared by analysis of variance (ANOVA) with level of significance set at 0.05 and two-tailed p values.

Results

The experimental paradigm for dual-reporter experiments is outlined in Fig. 1a. Details of flow cytometric analyses are given in Suppl. Fig. S 1 (Online Resource 9). Briefly, Csf1r-EGFP transgenic mice [62] were lethally irradiated and transplanted with DsRed-transduced wild-type BM (WT^{DsRed} → MacGreen BM chimeras). At 4 weeks after reconstitution, mice were subjected to 30 min MCAo/reperfusion. This approach permits distinction between resident microglia and invaded cells based on the differential expression of EGFP and DsRed. Shortly before MCAo, blood was obtained for flow cytometric analysis. We did not detect any residual EGFP$^+$ cells that could have subsequently invaded the ischemic brain. The percentages of DsRed$^+$ cells in circulating granulocytes, monocytes, and lymphocytes before MCAo are summarized in Suppl. Fig. S. 1a, b (Online Resource 9).

Next, we investigated the characteristics of circulating DsRed$^+$ white blood cells at 7 days after MCAo, the time

at which mice were killed for the electrophysiological and genomic analyses described below ($n = 10$ WT^{DsRed} → MacGreen BM chimeras). The FACS gating strategy is presented in Suppl. Fig S. 1c (Online Resource 9). This experiment confirmed that DsRed$^+$ cells, but not EGFP$^+$ cells, are present in all three white blood cell populations after stroke. A detailed analysis of circulating DsRed$^+$ monocytes revealed that $52 \pm 24\%$ were Cd11b$^+$ Ly6C^{hi} and $11 \pm 5\%$ were CD11b$^+$ Ly6C^{lo} (DsRed$^+$ granulocytes: $91 \pm 7\%$ Ly6G$^+$ CD11b$^+$ [polymorphonuclear granulocytes]; DsRed$^+$ lymphocytes: $23 \pm 15\%$ CD19$^+$ [B cells], $38 \pm 12\%$ CD3$^+$ [T cells], and $0.05 \pm 0.2\%$ CD335$^+$ [NK cells]). The population of Ly6C^{hi} monocytes has previously been shown to dominate the inflammatory infiltrate after brain infarction [20].

BM-derived monocytic cells adopt an activated morphology after brain ischemia

Immunohistological analysis on day 7 after 30 min MCAo/reperfusion showed that the contralateral (i.e., non-lesioned) hemisphere did not contain any DsRed-labeled cells (Fig. 1b). Furthermore, the contralateral hemisphere only contained surveying microglia showing a typical ramified morphology. By contrast, we found numerous DsRed$^+$ cells as well as EGFP$^+$ cells within the ipsilateral middle cerebral artery (MCA) territory. These cells typically showed an activated morphology with thickening and retraction of branches (Fig. 1c–e). Approximately 92% of DsRed$^+$ cells in the ischemic striatum displayed Iba1 immunoreactivity (138 out of 150 randomly selected DsRed$^+$ cells from three different animals; Fig. 1e). Furthermore, all EGFP$^+$ cells in the ischemic striatum showed Iba1 co-labeling.

Invading monocytic cells display an activated electrophysiological phenotype

Next, we analyzed the physiologic properties of EGFP$^+$ and of DsRed$^+$ cells in acute brain slices 1 week after MCAo/reperfusion. The contralateral hemisphere served as control. EGFP$^+$ cells in the non-ischemic brain ($n = 17$) showed the typical ramified morphology of resting microglia. By contrast, EGFP$^+$ cells ($n = 33$) and invaded DsRed$^+$ cells ($n = 13$) in the infarct zone displayed characteristic ameboid morphologies (Fig. 2a, upper panel). Patched cells which showed a stable seal were dialyzed with Alexa Fluor® 594 dye and imaged via a digital camera (Fig. 2a, bottom panel). EGFP$^+$ cells in the contralateral hemisphere displayed the typical current pattern previously described for resting microglia in acute slices [6]. De- and hyperpolarizing voltage steps elicited only small currents with an almost linear current voltage curve (Fig. 2b, c, left panel). EGFP$^+$ cells located in the stroke area showed inward rectifying currents with hyperpolarizing voltage steps with increasing
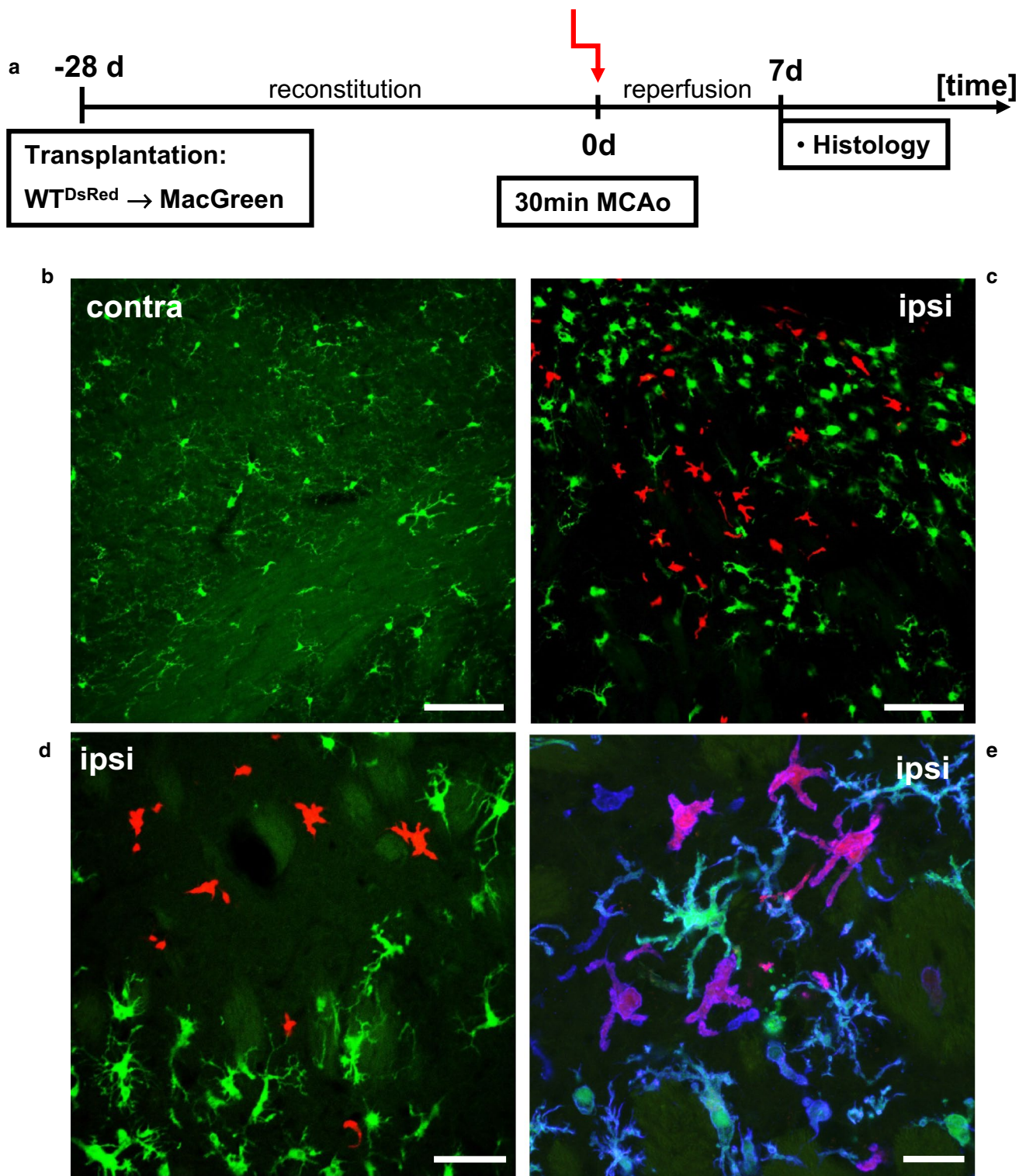
Fig. 1 Phenotypic characterization of WT[DsRed] → MacGreen BM chimeras 7 days after mild brain ischemia. **a** Experimental paradigm, **b** No DsRed^{+} cells were detected in the contralateral non-ischemic hemisphere. **c–e** Engraftment of BM-derived cells (red) in the ischemic striatum. Green: resident microglia. Blue (in **e**) microglia marker Iba1. Scale bar (in **b**, **c**) 100 μm, (in **d**) 50 μm, (in **e**) 20 μm

inactivation at more negative potentials and only small currents with depolarizing voltage steps comparable to cultured microglial cells ([32]; Fig. 2b, c, middle panel). The invading red fluorescent cells also exhibited the inward rectifying current, but additionally depolarizing voltage steps activated a delayed rectifying outward K^+ current. This current profile is typical of LPS-activated microglia and of peritoneal macrophages in vitro [31, 46, 47] and is seen transiently in activated microglia in situ after facial nerve axotomy [6]. Figure 2c shows current profiles and the corresponding I–V curves for a holding potential of − 70 mV.

Input membrane resistance in resting microglia in the contralateral non-ischemic hemisphere was significantly elevated as compared to EGFP$^+$ and DsRed$^+$ cells in the infarcted MCA territory (Fig. 2d). Interestingly, Rm also differed significantly between EGFP$^+$ and DsRed$^+$ cells in the ischemic brain, with the lowest Rm values recorded for DsRed$^+$ cells. Moreover, significant differences in membrane capacitance (Cm; Fig. 2e) and membrane potential (U; Fig. 2f) were observed between EGFP$^+$ cells in the ischemic lesion on the one hand and both DsRed$^+$ cells and contralateral EGFP$^+$ cells on the other hand. Finally, Fig. 2g summarizes outward and inward conductances normalized to membrane capacitance. Note that the specific outward conductance (Fig. 2g) was significantly higher in invaded DsRed$^+$ cells as compared to activated resident microglia.

Expression profiling reveals unique genomic signatures in microglia and invaded monocytic cells in the ischemic lesion

We hypothesized that functional differences between resident microglia and invaded monocytes should be mirrored in distinct transcriptomic profiles. To address this question, gene expression analysis was performed using ex vivo resident microglia and invaded monocytes isolated from the ischemic lesion on day 7 after MCAo (Fig. 3a–c). Four experiments were performed, each consisting of 4–7 WT^{DsRed} → MacGreen BM chimeras (Fig. 3a). As illustrated in Fig. 3c, cells from the ischemic lesion pre-enriched for CD11b could be easily subdivided into two distinct subsets: CD11b$^+$ EGFP$^+$ PI$^-$ microglia and CD11b$^+$ DsRed$^+$ PI$^-$ invading cells. Each experiment (denoted by the colors yellow, orange, blue, and black; Fig. 3b) yielded at least 50,000 EGFP$^+$ and 50,000 DsRed$^+$ cells for genomic analysis (see below). To further characterize the precise cellular composition of these EGFP$^+$ and DsRed$^+$ cells, we conducted an additional separate flow cytometry experiment (Suppl. Fig. S1d, Online Resorce 9). Investigation of CD11b$^+$ EGFP$^+$ cells revealed that $85.6 \pm 1.2\%$ were CD45^{lo} and $12.8 \pm 1.1\%$ were CD45^{hi}. Investigation of CD11b$^+$ DsRed$^+$ cells revealed that $66.7 \pm 4.5\%$ were CD45^{hi} and $25.9 \pm 4.3\%$ were CD45^{lo}.

We did not detect CD11b$^+$ DsRed$^+$ cells expressing CD3, CD335, or Ly6G. However, most of the CD11b$^+$ DsRed$^+$ cells ($64.6 \pm 4.7\%$) expressed Ly6C. Taken together, the population of CD11b$^+$ EGFP$^+$ cells is highly homogenous. Moreover, the population of CD11b$^+$ DsRed$^+$ cells displays considerable homogeneity. In particular, we did not detect expression of typical markers for T cells, NK cells, or polymorphonuclear granulocytes.

An impression of inter-sample similarity and variability is obtained by comparison of the different samples to each other by a correlation analysis. As basis for this analysis, the background-corrected normalized log2 intensity data were used (Fig. 3d). Considering that these data were obtained from amplified material, we found high correlation coefficients when the four samples derived from EGFP$^+$ cells were compared with each other (correlation coefficient > 0.94). Similarly, correlations between the corresponding four samples derived from DsRed$^+$ cells were also high (> 0.88). Euclidian distance analysis confirmed that EGFP$^+$ samples and DsRed$^+$ samples form different clusters (dendrogram in Fig. 3d).

Next, we performed a discriminatory analysis to identify genes differentially expressed in the two cell types after stroke (Fig. 3e, f). We detected 472 transcripts for DsRed > EGFP as well as 970 transcripts for EGFP > DsRed. In line with previous reports on differential gene expression between BM-derived macrophages and resident microglia, the category DsRed > EGFP contained *Ccr2* (e.g., [26, 40]) and the MYB transcription factor family member *Mybl2* [4, 22, 64] while EGFP > DsRed contained *Cx3Cr1* (e.g., [7, 42]). The results of the discriminatory analyses are given in Suppl. Tables S. 1 and S. 2 (Online Resource 1 and 2).

Subsequently, a functional grouping analysis was conducted to provide an overview of the different biological processes and pathways associated with the candidate genes identified above. Functional grouping may be highly suggestive, but, on its own, it does not provide definitive evidence of function. The bar graphs in Fig. 4a, b show how many reporters of the input reporter set were assigned to a specific biological category. Note that the size of the bars does not necessarily indicate a particular biological significance or over-representation since highly populated categories may simply arise due to the fact that these categories contain a higher number of genes. The tables in Fig. 4a, b provide the significance of an enrichment of the identified categories (Fisher's exact test with Benjamini–Hochberg correction for multiple testing). Values of $p \leq 0.05$ indicate a significant enrichment of the respective category relative to the background (all reporters of the Agilent Whole Mouse Oligo Microarrays 8 × 60K V2 with a Gene ID [Entrez]).

The results of the additional annotation enrichment analyses are displayed in Suppl. Tables S. 3 and S. 4
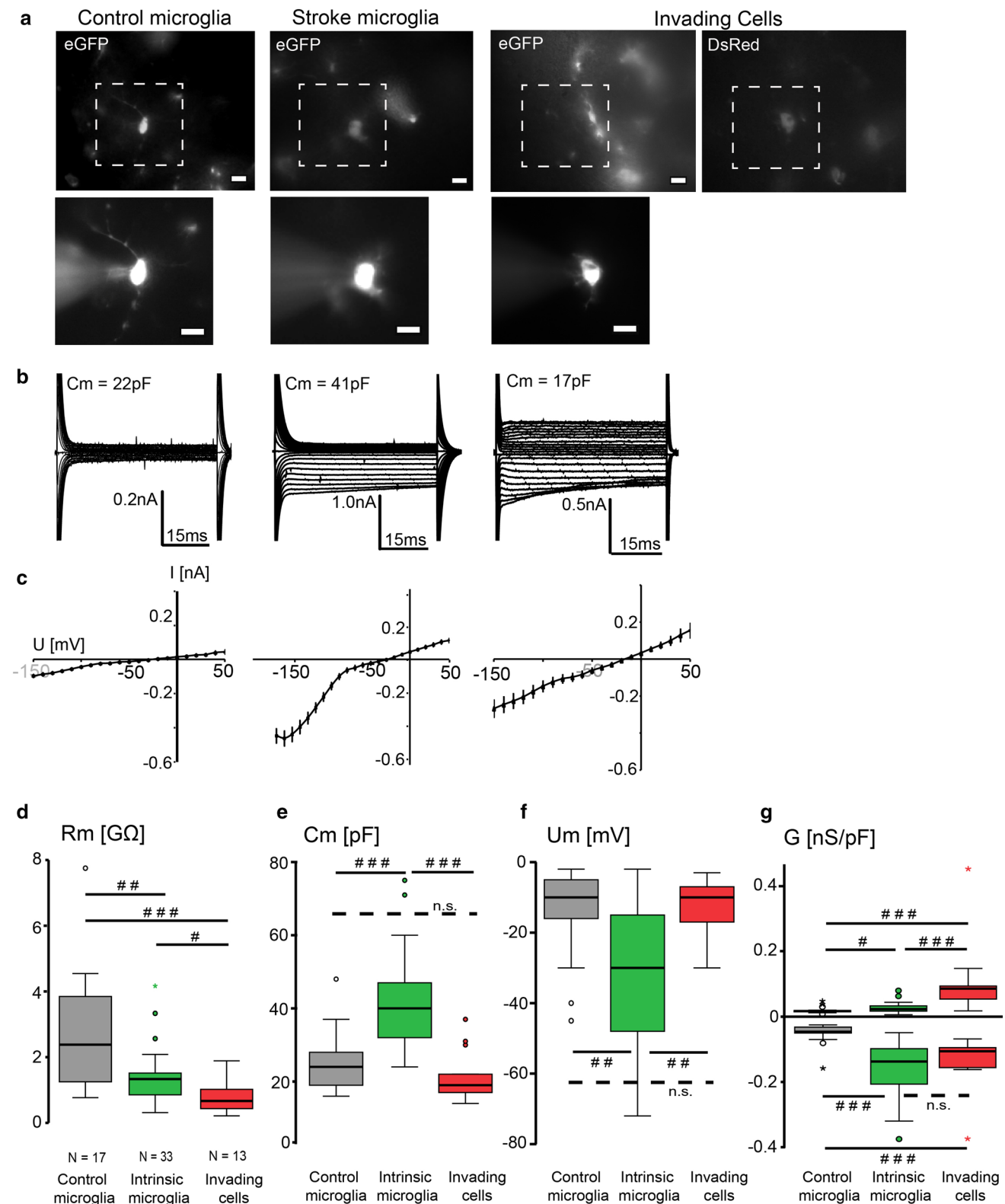
(Online Resource 3 and 4). In a nutshell, categories related to cell adhesion, immune processes, cell development and morphogenesis, ion transport, response to external stimuli, cell activation, response to stress, cell aging and other biological processes as well as categories related to neurons were significantly enriched in the candidate genes for EGFP > DsRed. The candidate genes with higher expression in DsRed-labeled cells show a high enrichment of

◄Fig. 2 Electrophysiological properties of intrinsic microglia and invading monocytic cells after mild brain ischemia. **a** Fluorescent images of EGFP$^+$ and DsRed$^+$ cells. Note the typical ramified morphology of resting microglia in the contralateral hemisphere (left) and the ameboid morphology of EGFP$^+$ and DsRed$^+$ cells in the infarcted MCA territory. The lower panel shows the recorded cells dialyzed with Alexa 594. All scale bars: 10 μm. **b** Membrane currents from the cells shown in **a** recorded in response to de- and hyperpolarizing voltage steps from − 150 mV to + 50 mV for 50 ms at a holding potential of − 70 mV. DsRed$^+$ cells showed an additional delayed rectifying outward K$^+$ current compared to EGFP$^+$ cells in the infarct. **c** I–V plots of average currents from all recordings obtained from EGFP$^+$ cells in the contralateral hemisphere ($n = 17$) and in the ischemic brain ($n = 33$) as well as from invaded DsRed$^+$ cells ($n = 13$). **d** Median input membrane resistance (Rm), calculated as Rm = U/I_{offset}. **e** Membrane capacitance (Cm) was calculated as Cm = $\int I \times \mathrm{d}t/\Delta U$, measuring with TIDA software the transient currents evoked in response to a depolarizing + 10 mV step from a holding potential of − 70 mV (50 ms). **f** Median membrane potential (Um [mV]) for the three cell types. **g** Box plots of outward and inward conductance normalized to membrane capacitance. Outward conductance was determined between 0 and − 20 mV, inward conductance between − 100 and − 120 mV and averaged for control microglia ($n = 17$), stroke-associated resident microglia ($n = 19$) and DsRed$^+$ cells ($n = 13$). #$p < 0.05$, ##$p < 0.005$, ###$p < 0.001$, Mann–Whitney U test

categories associated with cell stimulation, cell development and morphogenesis, the immune response, cell signaling (nucleotide) catabolic processes, cell adhesion, cell junction, cell death, and regulation of cell proliferation. A group of Killer cell lectin-like receptor genes (*Klra2*, *Klra6*, *Klra8*, *Klra9*) show a strong and partially exclusive expression in the DsRed samples as compared to the EGFP samples. Certain categories (e.g., cell development, response to wounding, inflammatory response, cell adhesion, and cell activation) were returned for both lists, but are associated with different sets of transcripts. For example, the term 'chemotaxis' includes the chemokines *Ccl3*, *Ccl4*, *Cxcl13*, and *Cxcl17* for EGFP > DsRed, and *Ccl17* and *Ccl22* for DsRed > EGFP.

The M1/M2 classification remains a useful heuristic paradigm, although it clearly does not do sufficient justice to the full spectrum of macrophage polarization under disease conditions in vivo. Figure 4c, d summarizes the comparison of key M1- and M2-associated genes between microglia and invaded macrophages. While this comparison did not yield a clear dichotomous pattern between the two cell types after brain ischemia, more subtle differences were still apparent. On the whole, and compared to resident microglia, gene expression in invading monocytes seems to be less skewed toward the M1 phenotype and more skewed toward the M2 phenotype.

As a further step, the differentially regulated transcripts (Suppl. Tables S. 1 and S. 2, Online Resource 1 and 2) were collated with a published transcriptome database for genes enriched by at least 1.5-fold in oligodendrocytes, astrocytes,

and neurons [8]. This stringent comparison yielded 337 transcripts specifically expressed in invaded macrophages (Suppl. Table S. 5, Online Resource 5) and 771 transcripts specifically expressed in microglia (Suppl. Table S. 6, Online Resource 6). These unique gene sets offer an exciting new window on the biology of microglia and blood-derived macrophages in the pathogenesis of ischemic stroke.

Next, we compared our results, which represent the first detailed transcriptomic analysis of monocytes and microglia in brain ischemia published to date, to a roster of microglia-specific genes recently identified by Butovsky and co-workers [7]. Importantly, the 152 genes identified in that study were derived from an analysis of microglia and CD11b$^+$ Ly6C$^+$ monocyte subsets harvested from intact adult mice [7]. None of these 152 microglia-specific genes was found in our DsRed > EGFP dataset. In contrast, our EGFP > DsRed dataset contains 56 transcripts previously identified by Butovsky et al. (Suppl. Table S. 7, Online Resource 7). A list of the microglia-specific transcripts newly identified in this report and not described by Butovsky et al. [7] is also provided in Suppl. Table S. 7 (Online Resource 7). Finally, a comparison of our findings with microglia-enriched molecules in an autoimmune encephalomyelitis model [7] also yielded a high overlap of identified transcripts (~ 40%; Suppl. Table S. 8, Online Resource 8) with our EGFP > DsRed dataset—a striking finding considering that gene expression in that study was investigated at the time of disease onset whereas we here focused on a delayed time point after MCAo, an entirely different injury model.

Diminished engraftment of myeloid cells exacerbates ischemic injury

P-selectin glycoprotein ligand-1 (PSGL-1; encoded by the gene Selplg) is the high-affinity counter-receptor for P-selectin on myeloid cells. It plays a crucial role in mediating the initial capture (i.e., 'rolling') of leukocytes on the endothelial surface at the site of inflammation (e.g., [53, 66]). Several experimental reports have demonstrated that PSGL-1 is critical to monocyte homing and transmigration into inflamed tissue [3, 35]. In an attempt at a functional characterization of how blood-borne cells shape stroke outcome, we used BM harvested from Selplg-KO and Selplg-WT mice to create BM chimeras (Selplg-KO$^{\text{EGFP}}$ → WT and Selplg-KO$^{\text{DsRed}}$ → WT chimeras along with the corresponding controls; Fig. 5a). Acute lesion sizes as assessed on MR imaging at 48 h after MCAo did not differ significantly between chimeras with Selplg-WT and Selplg-KO BM (33 ± 8.3 vs. 41 ± 5.4 mm^3, $n = 5$–9 animals per group, $p > 0.05$). Histological outcome was assessed on day 7 after 30 min MCAo/reperfusion. The number of transduced cells in the ischemic striatum was strongly reduced in Selplg-KO$^{\text{EGFP}}$ → WT chimeras as compared to Selplg-WT$^{\text{EGFP}}$ → WT chimeras (cells
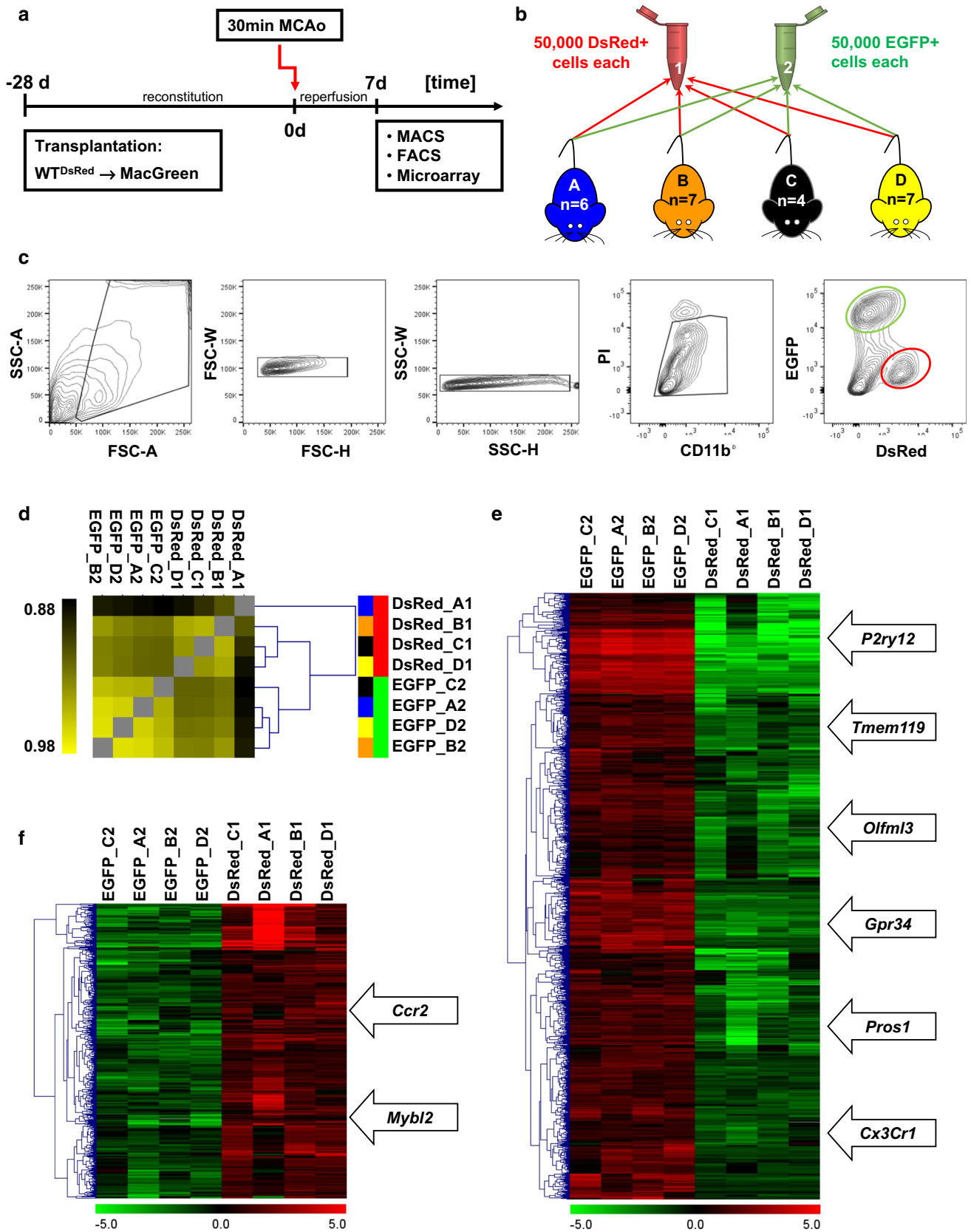
◀**Fig. 3** Resident microglia and invading macrophages show different genomic profiles after mild brain ischemia. **a** Experimental setup. **b** The four colors (blue, orange, black and yellow) represent the four different experimental groups, each consisting of 4–7 WT^{DsRed} → MacGreen BM chimeras subjected to MCAo. **c** Flow cytometry gating strategy of MACS-purified CD11b$^+$ cells from the ischemic brain. Cells were sorted for CD11b$^+$ EGFP$^+$ PI$^-$ and CD11b$^+$ DsRed$^+$ PI$^-$ cells **d** Interexperiment correlation analysis of normalized log2 intensities of all samples. The correlation matrix was clustered using Euclidean distance metric. Color saturation limits were set from 0.88 to 0.98, as indicated by the gradient bar to the left of the graph. The tree structure next to the heatmap indicates clusters of samples according to their degree of similarity. **e**, **f** Clustered heatmap (Euclidean distance, complete linkage) showing reporters according to the selection criteria EGFP > DsRed (**e**) and DsRed > EGFP (**f**). FSC forward scatter, SSC sideward scatter, PI propidium iodide

per μm^3: 3410 ± 1137 vs. 5651 ± 1787; $p = 0.046$, $n = 9$–10 animals per group; Fig. 5b). Independent of the genotype of the donor BM, almost all EGFP-transduced cells invading the infarct displayed Iba1 immunoreactivity (Selplg-WT^{EGFP} → WT chimeras: $92 \pm 2\%$; Selplg-KO^{EGFP} → WT chimeras: $88 \pm 2\%$; $n = 4$ randomly selected animals per group; Fig. 5c). The reduced invasion of blood-derived cells was accompanied by significantly increased lesion volumes in Selplg-KO^{EGFP} → WT chimeras (Fig. 5d, e).

In a separate set of experiments, we studied sensorimotor performance after stroke using the rotorod test and the pole test. Sensorimotor performance in sham-operated mice did not differ between Selplg-KO^{DsRed} → WT chimeras and Selplg-WT^{DsRed} → WT chimeras (Fig. 5f, g). However, after stroke, significant differences emerged between genotypes with Selplg-KO^{DsRed} → WT chimeras being more severely affected (Fig. 5f, g).

Finally, to assess whether PSGL-1 deficiency impacts key characteristics of invading cells in our stroke model, we performed a detailed transcriptomic analysis of retrovirally transduced CD11b$^+$ CD45^{hi} cells harvested from the ischemic brain at 7 days after MCAo (Suppl. Fig. S. 2a–c, Online Resource 10; GEO accession: GSE105011). Samples derived from Selplg-KO^{DsRed} → WT chimeras and Selplg-WT^{DsRed} → WT chimeras did not segregate into different clusters (Suppl. Fig. S. 2b, Online Resource 10). Moreover, mRNA expression of key M1 and M2 genes did not differ significantly between samples (Suppl. Fig. S. 2d, Online Resource 10). All told, these findings point to the conclusion that increased lesion sizes in BM chimeras lacking Selplg become apparent during the course of the first week after MCAo. Most probably, increased lesion sizes in Selplg-KO chimeras are not due to changes in the behavior of invaded cells in the ischemic brain, in particular as relates to polarization, but simply reflect the effects of overall reduced numbers of invading cells.

Discussion

This study yielded the following key results: (1) For the first time, we describe distinguishing molecular signatures for resident microglia and invading monocytes after brain ischemia. Functional categories significantly enriched in monocytes include cell migration, cell proliferation, and calcium signaling, indicative of strong activation. (2) The electrophysiological properties of resident microglia and invading monocytes differ in the ischemic brain with the latter displaying an additional delayed rectifying outward K$^+$ current. (3) We show that reduced invasion of monocytes into the ischemic brain exacerbates stroke outcome.

In this study, we set out to dissect the pathogenetic roles of resident microglia and invaded monocytes in ischemic stroke. Our well-characterized model of mild transient brain ischemia is particularly well suited to elucidate similarities and differences in the effector phenotypes of these two myeloid cell populations: The 30-min ischemic episode produces delayed and selective neuronal death. In contrast, glial cells including microglia are left intact [29, 34]. Furthermore, mortality is low and histological outcome (i.e., lesion size) is easily and reliably determined [15, 80]. Given that we focused on a single, relatively late time point after mild ischemic brain infarction, we caution that our results reflect microglia and monocyte behaviors during the delayed phases of post-stroke regeneration and may not be broadly generalizable. An additional methodical caveat concerns the use of BM chimeras in this report versus the use of other experimental models (e.g., purely genetic models, parabiosis, etc.) in a number of earlier studies [7, 36, 79]. In this regard, the finding of an enrichment of genes involved in proliferation in the DsRed-labeled monocyte-derived macrophages compared to the EGFP-labeled microglia is remarkable, since microglia are known to proliferate in response to injury [23, 36, 44, 55]. However, one possible explanation for this unexpected observation may relate to the fact that, in the set of experiments reported here, we used whole-body-irradiated mice without head shielding, which show a significant reduction in both baseline and lesion-induced microglial proliferation [77].

Here, we used acute brain slices to investigate the physiological properties of intrinsic microglia and invading monocytes after brain ischemia. Converging evidence from experimental studies and human stroke specimens indicates that mild ischemia/reperfusion, in particular, either does not lead to any appreciable extravasation of circulating polymorphonuclear granulocytes into the brain parenchyma [13] or, alternatively, that even if these cells cross the laminin barrier, they still remain in intimate proximity to the neurovascular unit [71]. In the electrophysiological experiments, the morphology of patched
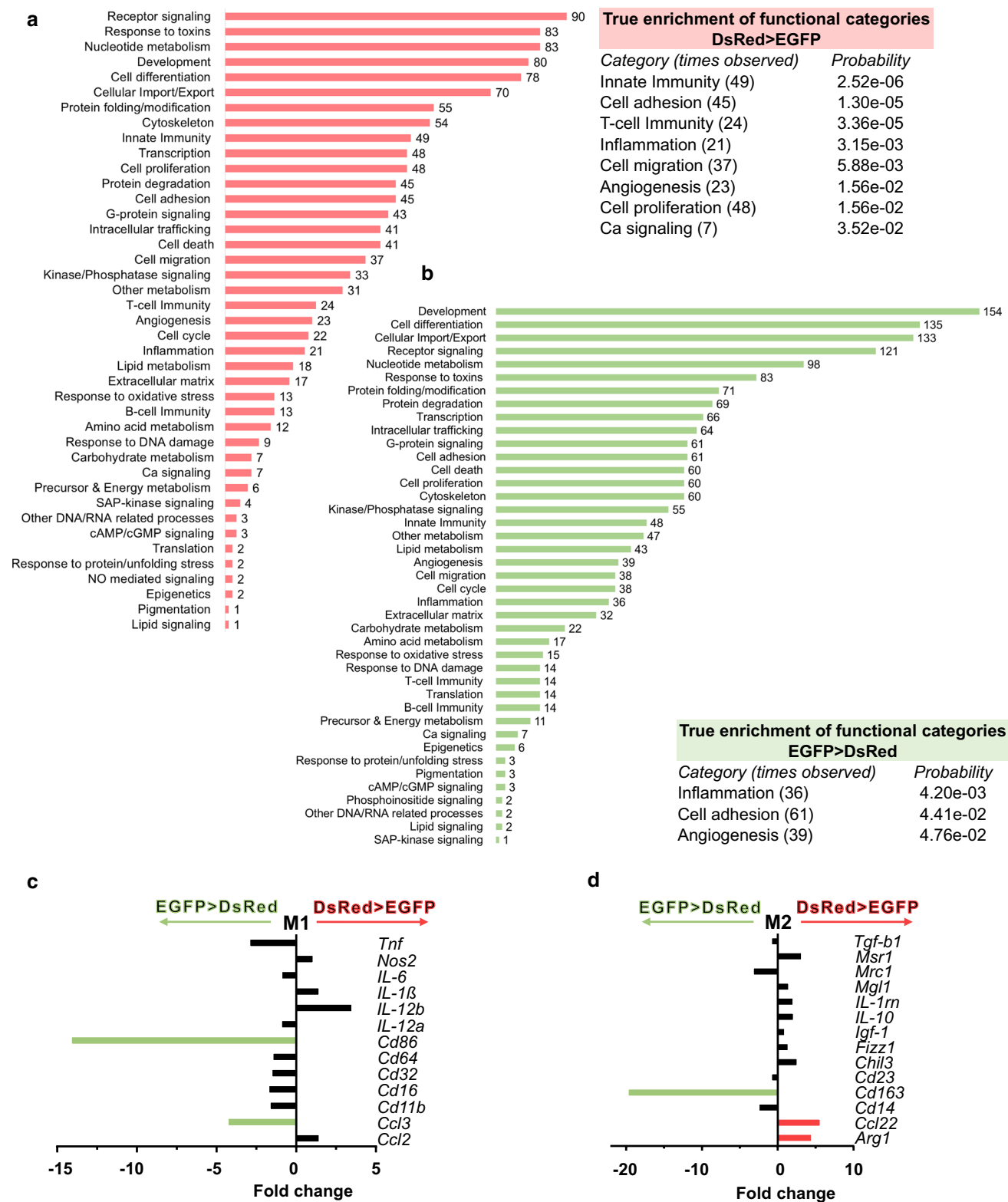
Fig. 4 Functional grouping analysis. **a**, **b** Functional grouping analysis for the list of differentially expressed genes DsRed > EGFP (**a**) and EGFP > DsRed (**b**). The bar graphs indicate how many genes are assigned to the different categories. The table represents the significance of an enrichment of the identified categories. **c**, **d** Compar-

ison of the expression levels of key M1- (**c**) and M2-associated (**d**) genes between microglia and invaded macrophages. Differentially regulated genes identified in our discriminatory analysis (Suppl. Tables S. 1 and S. 2, Online Resource 1 and 2) are highlighted in red (DsRed > EGFP) or green (EGFP > DsRed)
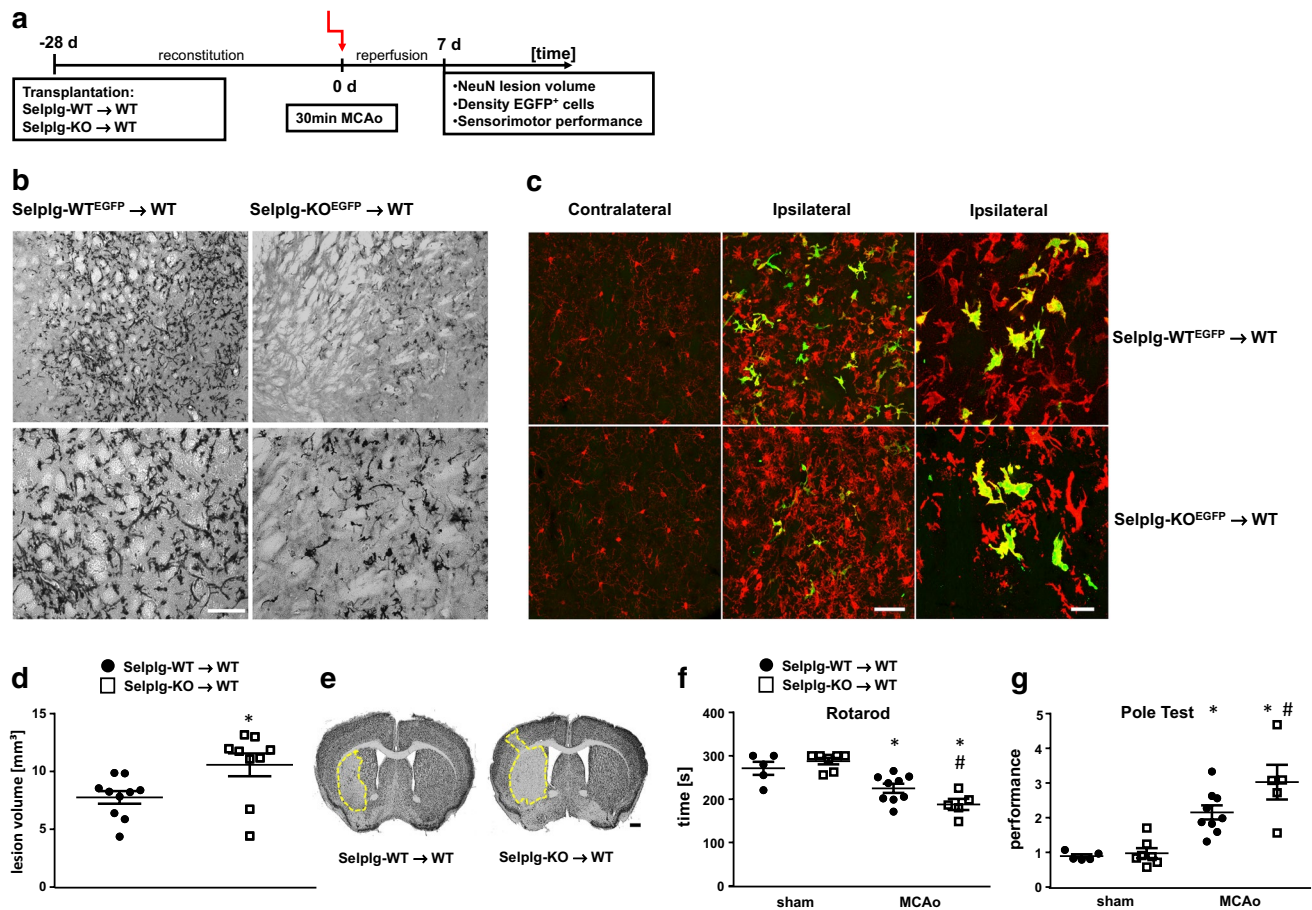
Fig. 5 Reduced recruitment of myeloid cells into the ischemic brain results in poorer stroke outcome. **a** Experimental setup. **b** Reduced engraftment of EGFP-transduced cells in Selplg-KO^EGFP → WT chimeras as compared to Selplg-WT^EGFP → WT chimeras. White scale bar (shown in lower panel) 100 μm in lower panel, 200 μm in upper panel. **c** EGFP-transduced cells invading the infarcted brain acquire Iba1 immunoreactivity (red). Scale bar (middle panel) 50 μm in left and middle panels, scale bar (right panel) 20 μm. **d** Neuronal damage was assessed 7 days after MCAo/reperfusion using NeuN immunohistochemistry. Lesion size was quantified using computer-assisted volumetry. $N = 9$–10 animals per group. $*p < 0.05$, unpaired Student's t test. **e** Representative images of NeuN-stained coronal brain sections at day 7 after 30 min MCAo. **f**, **g** Sensorimotor performance of Selplg-KO^DsRed → WT chimeras as compared to Selplg-WT^DsRed → WT chimeras was assessed using the rotarod (**f**) and the pole test (**g**). Post-stroke pole test performance was quantified according to the following equation: performance = mean time of post-stroke trials/mean time of baseline trials (higher values represent worse sensorimotor abilities post-stroke). Two-way ANOVA followed by post hoc test. $N = 5$–9 animals per group. $*p < 0.05$ relative to the respective sham controls; $\#p < 0.05$ between the two MCAo groups

cells was carefully examined using phase-contrast microscopy to ensure, if possible, the absence of cells with a multilobulated nucleus in the cytoplasm and of cells with characteristic granular structures [30]. Moreover, uncharacteristically small DsRed⁺ cells (< 10 μm) as well as DsRed⁺ cells with a high nuclear–cytoplasmic ratio were excluded. In line with earlier reports, intrinsic microglia cells from uninjured brain displayed a ramified morphology and lacked voltage-gated channels [6]. We did not detect any blood-derived cells in the contralateral non-ischemic hemisphere. Both microglia and invaded monocytes in the ischemic MCA territory displayed activated, ameboid morphologies at 7 days post-event. EGFP⁺ cells located in the stroke area showed an inward current profile

comparable to unstimulated microglia in culture [32] along with a very small outward current. The invading red fluorescent cells displayed an additional delayed rectifying outward K⁺ current characteristic of strong microglia activation such as occurs after LPS stimulation in vitro [46, 47] or transiently after facial nerve axotomy in situ [6]. Our study shows that the outward current of invading cells is maintained 7–9 days after stroke induction suggesting that these invading cells remain more highly activated than resident microglia during the subacute phase of stroke [37].

In our transcriptomic investigation, monocyte-derived phagocytes and resident microglia were essentially extracted from the same post-ischemic milieu. Our genomic findings

firmly establish that microglia and engrafted monocytes, which both transform into brain macrophages after ischemia/reperfusion, retain unique, distinguishing molecular signatures during the subacute phase of stroke. Crucially, more than a third of the top microglia genes previously identified by a comparison of microglia from the healthy brain and peripheral monocyte subsets [7] also emerged in our dataset for EGFP > DsRed after stroke. However, further exploration, in particular, of the microglia transcripts newly identified in this report (such as *Naalad2*, *Prkca, Klk8,* and many others) may prove even more useful in pointing toward novel and specific functions of effector microglia in stroke biology. For example, the exclusive expression of *Naalad2* (N-acetylated alpha-linked acidic dipeptidase 2) links microglia with *N*-acetyl-*L*-aspartyl-*L*-glutamate (NAAG), which is among the most prevalent neurotransmitters in the mammalian brain. Furthermore, Naaladase enzymes represent druggable targets that have recently garnered interest for indications such as traumatic brain injury, spinal cord injury, and Alzheimer's disease [81]. Protein kinase C alpha (encoded by the *Prkca* gene) is a versatile member of the protein kinase family of enzymes implicated in a great variety of cellular functions [43]. Equally interestingly, kallikrein 8 (encoded by *Klk8*) has so far been implicated in neuroinflammation and disease progression in multiple sclerosis (e.g., [49]).

Interestingly, the candidate genes with higher expression in EGFP+ cells than in DsRed+ cells show a significant enrichment of categories related to neurons. Here, it must be stressed that our methodology for cell isolation was rigorous, involving sequential rounds of MACS and FACS including a successive gating strategy to assure that doublets and debris were faithfully eliminated. We again find, in our dataset obtained from cell type-specific high-quality mRNA from ischemic brain tissue, a high number of those genes that have previously been identified as top microglia/neuron genes in uninjured brain (*Tanc2*, *Rgmb*, *Npnt*, *Rtn4rl1*, *Khdrbs3*, *Rtn1*; [7]). What might be the pathobiological significance of this enrichment of neuronal genes in microglia-derived macrophages? During development, microglia phagocytose neurons undergoing programmed cell death [51]. Moreover, microglia play a major role in sculpting synaptic connections by actively disposing of synaptic material [50]. Furthermore, an age-associated reduction in the neuronal mRNA content of microglia was recently reported in the human brain [14]. Taken together with these earlier reports, our findings suggest that, in the context of post-stroke recovery, the task of clearing neuronal debris falls primarily on microglia-derived macrophages.

The most salient observation from our electrophysiological characterization, namely that blood-derived macrophages are in certain ways more strongly activated than the resident microglia population in the infarct, aligns well with the results of gene expression profiling. Outward K+

conductances, in particular, are functionally linked to activation parameters such as cell migration, cell proliferation, and intracellular calcium [45, 48, 68, 73]. Remarkably, these categories also emerged from the functional grouping analysis of the gene set DsRed > EGFP (Fig. 4a). Furthermore, nucleotide catabolism is one of the key functional categories identified in the annotation enrichment analysis of the transcripts upregulated in blood-derived brain macrophages (Suppl. Table S. 3, Online Resource 3), a finding which fits well with the observation in microglia that purinergic signaling is required for outward K+ currents in response to neuronal injury [68]. Future work will have to confirm differential expression of key molecules within these broad functional categories at the protein level.

Finally, a number of experimental studies have described beneficial effects of monocyte-derived macrophages on murine stroke outcome [9, 19, 75]. Blocking monocyte recruitment using an anti-CCR2 antibody during the first week after stroke abolished recovery [75]. Similarly, selective CCR2 antagonism decreased the number of Ly6C^hi monocytes infiltrating the ischemic brain and led to increased infarct sizes [9]. Our complementary approach using chimeras reconstituted with donor BM harvested from Selplg-KO mice allowed us to reliably and strongly decrease the invasion of blood-borne cells into the ischemic brain with the added bonus of avoiding some of the side effects of a pharmacological blockade of the CCL2–CCR2 signaling axis (e.g., blockade of monocyte migration into other organs, binding to other cell types such as T cells, and off-target activity; reviewed in [5, 63, 69]). In line with the studies cited above [9, 19, 75], our approach also yielded increased infarct sizes and worsened sensorimotor performance in chimeras with Selplg-deficient BM after stroke. Importantly, a further transcriptomic investigation of the invaded cells in the ischemic brain did not reveal significant differences in polarization between cells derived from Selplg-KO and Selplg-WT BM. We conclude that increased lesion volumes in Selplg-KO → WT chimeras at 7 days mainly reflect the effects of an overall decrease in the number of infiltrating cells.

As a surprising aside, we should note that Selplg was one of the genes detected in our dataset EGFP > DsRed. The importance of PSGL-1 for leukocyte recruitment into inflamed tissue has been appreciated for a long time [38, 66]. By contrast, little is known about the function of PSGL-1 in microglia. Only recently was Selplg identified as an important microglial 'sensome' gene [27]. It can be presumed that ligand binding to PSGL-1 represents a microglia alarm signal. For example, bacterial ligands for PSGL-1 have been identified of late [57]. It should be noted that the fact that Selplg is contained in the category EGFP > DsRed may also be due to reduced Selplg mRNA transcription in infiltrated DsRed+ cells at 7 days

after MCAo. Indeed, there is some evidence to indicate that activated monocytes and macrophages downregulate Selplg (NCBI Gene Expression Omnibus; GSE69607, GSE28621 and GSE69607).

One should be careful not to generalize about a complex subject such as microglia/macrophage polarization on the basis of transcriptomic profiles. However, it is still interesting to note that our gene expression analysis at 7 days after MCAo suggests that, generally speaking, invading monocytes might be more skewed toward an M2 phenotype than resident microglia. In addition, our discriminatory analysis yielded two M2 genes in the dataset DsRed > EGFP (*Arg1* and *Ccl22*). Interestingly, arginase-1 expression in invading monocytes has also recently been demonstrated at the protein level [41]. At the same time, no typical M1 gene was detected in the gene set DsRed > EGFP. On balance, based on our experiments, neither invading monocytes nor microglia can sufficiently be described with just one single activation state. Although clearly distinct from each other, both display a mixture of known phenotypes which points to the significance of as yet undefined 'intermediate states' observed under disease conditions in vivo.

In summary, our study establishes crucial differences in activation state between resident microglia and invading macrophages after stroke and identifies unique molecular signatures for either cell type. Our findings provide novel insights into the biology of myeloid cells in the ischemic brain and highlight the possibility of targeting monocytes to improve stroke outcome.

Compliance with ethical standards

Conflict of interest The authors declare no competing financial interests.

References

1. Ajami B, Bennett JL, Krieger C, Tetzlaff W, Rossi FM (2007) Local self-renewal can sustain CNS microglia maintenance and function throughout adult life. Nat Neurosci 10:1538–1543. https://doi.org/10.1038/nn2014
2. Alliot F, Godin I, Pessac B (1999) Microglia derive from progenitors, originating from the yolk sac, and which proliferate in the brain. Brain Res Dev Brain Res 117:145–152
3. An G, Wang H, Tang R, Yago T, McDaniel JM, McGee S, Huo Y, Xia L (2008) P-selectin glycoprotein ligand-1 is highly expressed on Ly-6Chi monocytes and a major determinant for Ly-6Chi monocyte recruitment to sites of atherosclerosis in mice. Circulation 117:3227–3237. https://doi.org/10.1161/CIRCULATIONAHA.108.771048
4. Baker SJ, Ma'ayan A, Lieu YK, John P, Reddy MV, Chen EY, Duan Q, Snoeck HW, Reddy EP (2014) B-myb is an essential regulator of hematopoietic stem cell and myeloid progenitor cell development. Proc Natl Acad Sci USA 111:3122–3127. https://doi.org/10.1073/pnas.1315464111
5. Bose S, Cho J (2013) Role of chemokine CCL2 and its receptor CCR2 in neurodegenerative diseases. Arch Pharmacal Res 36:1039–1050. https://doi.org/10.1007/s12272-013-0161-z
6. Boucsein C, Kettenmann H, Nolte C (2000) Electrophysiological properties of microglial cells in normal and pathologic rat brain slices. Eur J Neurosci 12:2049–2058
7. Butovsky O, Jedrychowski MP, Moore CS, Cialic R, Lanser AJ, Gabriely G, Koeglsperger T, Dake B, Wu PM, Doykan CE et al (2014) Identification of a unique TGF-beta-dependent molecular and functional signature in microglia. Nat Neurosci 17:131–143. https://doi.org/10.1038/nn.3599
8. Cahoy JD, Emery B, Kaushal A, Foo LC, Zamanian JL, Christopherson KS, Xing Y, Lubischer JL, Krieg PA, Krupenko SA et al (2008) A transcriptome database for astrocytes, neurons, and oligodendrocytes: a new resource for understanding brain development and function. J Neurosci 28:264–278. https://doi.org/10.1523/JNEUROSCI.4178-07.2008
9. Chu HX, Broughton BR, Kim HA, Lee S, Drummond GR, Sobey CG (2015) Evidence that Ly6C(hi) monocytes are protective in acute ischemic stroke by promoting M2 macrophage polarization. Stroke 46:1929–1937. https://doi.org/10.1161/STROKEAHA.115.009426
10. Djukic M, Mildner A, Schmidt H, Czesnik D, Bruck W, Priller J, Nau R, Prinz M (2006) Circulating monocytes engraft in the brain, differentiate into microglia and contribute to the pathology following meningitis in mice. Brain 129:2394–2403. https://doi.org/10.1093/brain/awl206
11. Edgar R, Domrachev M, Lash AE (2002) Gene Expression Omnibus: NCBI gene expression and hybridization array data repository. Nucleic Acids Res 30:207–210
12. Endres M, Meisel A, Biniszkiewicz D, Namura S, Prass K, Ruscher K, Lipski A, Jaenisch R, Moskowitz MA, Dirnagl U (2000) DNA methyltransferase contributes to delayed ischemic brain injury. J Neurosci 20:3175–3181
13. Enzmann G, Mysiorek C, Gorina R, Cheng YJ, Ghavampour S, Hannocks MJ, Prinz V, Dirnagl U, Endres M, Prinz M et al (2013) The neurovascular unit as a selective barrier to polymorphonuclear granulocyte (PMN) infiltration into the brain after ischemic injury. Acta Neuropathol 125:395–412. https://doi.org/10.1007/s00401-012-1076-3
14. Galatro TF, Holtman IR, Lerario AM, Vainchtein ID, Brouwer N, Sola PR, Veras MM, Pereira TF, Leite REP, Moller T et al (2017) Transcriptomic analysis of purified human cortical microglia reveals age-associated changes. Nat Neurosci 20:1162–1171. https://doi.org/10.1038/nn.4597

15. Gertz K, Kronenberg G, Kalin RE, Baldinger T, Werner C, Balkaya M, Eom GD, Hellmann-Regen J, Krober J, Miller KR et al (2012) Essential role of interleukin-6 in post-stroke angiogenesis. Brain 135:1964–1980. https://doi.org/10.1093/brain/aws075

16. Gertz K, Priller J, Kronenberg G, Fink KB, Winter B, Schrock H, Ji S, Milosevic M, Harms C, Bohm M et al (2006) Physical activity improves long-term stroke outcome via endothelial nitric oxide synthase-dependent augmentation of neovascularization and cerebral blood flow. Circ Res 99:1132–1140. https://doi.org/10.1161/01.RES.0000250175.14861.77

17. Ginhoux F, Greter M, Leboeuf M, Nandi S, See P, Gokhan S, Mehler MF, Conway SJ, Ng LG, Stanley ER et al (2010) Fate mapping analysis reveals that adult microglia derive from primitive macrophages. Science 330:841–845. https://doi.org/10.1126/science.1194637

18. Gliem M, Krammes K, Liaw L, van Rooijen N, Hartung HP, Jander S (2015) Macrophage-derived osteopontin induces reactive astrocyte polarization and promotes re-establishment of the blood brain barrier after ischemic stroke. Glia 63:2198–2207. https://doi.org/10.1002/glia.22885

19. Gliem M, Mausberg AK, Lee JI, Simiantonakis I, van Rooijen N, Hartung HP, Jander S (2012) Macrophages prevent hemorrhagic infarct transformation in murine stroke models. Ann Neurol 71:743–752. https://doi.org/10.1002/ana.23529

20. Gliem M, Schwaninger M, Jander S (2016) Protective features of peripheral monocytes/macrophages in stroke. Biochem Biophys Acta 1862:329–338. https://doi.org/10.1016/j.bbadis.2015.11.004

21. Gomez Perdiguero E, Klapproth K, Schulz C, Busch K, Azzoni E, Crozet L, Garner H, Trouillet C, de Bruijn MF, Geissmann F et al (2015) Tissue-resident macrophages originate from yolk-sac-derived erythro-myeloid progenitors. Nature 518:547–551. https://doi.org/10.1038/nature13989

22. Gomez Perdiguero E, Schulz C, Geissmann F (2013) Development and homeostasis of "resident" myeloid cells: the case of the microglia. Glia 61:112–120. https://doi.org/10.1002/glia.22393

23. Graeber MB, Streit WJ, Kreutzberg GW (1989) Formation of microglia-derived brain macrophages is blocked by adriamycin. Acta Neuropathol 78:348–358

24. Grathwohl SA, Kalin RE, Bolmont T, Prokop S, Winkelmann G, Kaeser SA, Odenthal J, Radde R, Eldh T, Gandy S et al (2009) Formation and maintenance of Alzheimer's disease beta-amyloid plaques in the absence of microglia. Nat Neurosci 12:1361–1363. https://doi.org/10.1038/nn.2432

25. Haas S, Brockhaus J, Verkhratsky A, Kettenmann H (1996) ATP-induced membrane currents in ameboid microglia acutely isolated from mouse brain slices. Neuroscience 75:257–261

26. Hammond MD, Taylor RA, Mullen MT, Ai Y, Aguila HL, Mack M, Kasner SE, McCullough LD, Sansing LH (2014) CCR2+ Ly6C(hi) inflammatory monocyte recruitment exacerbates acute disability following intracerebral hemorrhage. J Neurosci 34:3901–3909. https://doi.org/10.1523/JNEUROSCI.4070-13.2014

27. Hickman SE, Kingery ND, Ohsumi TK, Borowsky ML, Wang LC, Means TK, El Khoury J (2013) The microglial sensome revealed by direct RNA sequencing. Nat Neurosci 16:1896–1905. https://doi.org/10.1038/nn.3554

28. Ji S, Kronenberg G, Balkaya M, Farber K, Gertz K, Kettenmann H, Endres M (2009) Acute neuroprotection by pioglitazone after mild brain ischemia without effect on long-term outcome. Exp Neurol 216:321–328. https://doi.org/10.1016/j.expneurol.2008.12.007

29. Katchanov J, Harms C, Gertz K, Hauck L, Waeber C, Hirt L, Priller J, von Harsdorf R, Bruck W, Hortnagl H et al (2001) Mild cerebral ischemia induces loss of cyclin-dependent kinase inhibitors and activation of cell cycle machinery before delayed neuronal cell death. J Neurosci 21:5045–5053

30. Kawa K (1989) Electrophysiological properties of three types of granulocytes in circulating blood of the newt. J Physiol 415:211–231

31. Kettenmann H, Hoppe D, Gottmann K, Banati R, Kreutzberg G (1990) Cultured microglial cells have a distinct pattern of membrane channels different from peritoneal macrophages. J Neurosci Res 26:278–287. https://doi.org/10.1002/jnr.490260303

32. Kettenmann H, Ilschner S (1993) Physiological properties of microglia. Clin Neuropathol 12:306–307

33. Kilkenny C, Browne WJ, Cuthill IC, Emerson M, Altman DG (2010) Improving bioscience research reporting: the ARRIVE guidelines for reporting animal research. PLoS Biol 8:e1000412. https://doi.org/10.1371/journal.pbio.1000412

34. Kronenberg G, Wang LP, Synowitz M, Gertz K, Katchanov J, Glass R, Harms C, Kempermann G, Kettenmann H, Endres M (2005) Nestin-expressing cells divide and adopt a complex electrophysiologic phenotype after transient brain ischemia. J Cereb Blood Flow Metab 25:1613–1624. https://doi.org/10.1038/sj.jcbfm.9600156

35. Leon B, Ardavin C (2008) Monocyte migration to inflamed skin and lymph nodes is differentially controlled by L-selectin and PSGL-1. Blood 111:3126–3130. https://doi.org/10.1182/blood-2007-07-100610

36. Li T, Pang S, Yu Y, Wu X, Guo J, Zhang S (2013) Proliferation of parenchymal microglia is the main source of microgliosis after ischaemic stroke. Brain 136:3578–3588. https://doi.org/10.1093/brain/awt287

37. Lyons SA, Pastor A, Ohlemeyer C, Kann O, Wiegand F, Prass K, Knapp F, Kettenmann H, Dirnagl U (2000) Distinct physiologic properties of microglia and blood-borne cells in rat brain slices after permanent middle cerebral artery occlusion. J Cereb Blood Flow Metab 20:1537–1549. https://doi.org/10.1097/00004647-200011000-00003

38. McEver RP, Cummings RD (1997) Perspectives series: cell adhesion in vascular biology. Role of PSGL-1 binding to selectins in leukocyte recruitment. J Clin Investig 100:485–491. https://doi.org/10.1172/JCI119556

39. Mildner A, Mack M, Schmidt H, Bruck W, Djukic M, Zabel MD, Hille A, Priller J, Prinz M (2009) CCR2+ Ly-6Chi monocytes are crucial for the effector phase of autoimmunity in the central nervous system. Brain 132:2487–2500. https://doi.org/10.1093/brain/awp144

40. Mildner A, Schmidt H, Nitsche M, Merkler D, Hanisch UK, Mack M, Heikenwalder M, Bruck W, Priller J, Prinz M (2007) Microglia in the adult brain arise from Ly-6ChiCCR2+ monocytes only under defined host conditions. Nat Neurosci 10:1544–1553. https://doi.org/10.1038/nn2015

41. Miro-Mur F, Perez-de-Puig I, Ferrer-Ferrer M, Urra X, Justicia C, Chamorro A, Planas AM (2016) Immature monocytes recruited to the ischemic mouse brain differentiate into macrophages with features of alternative activation. Brain Behav Immun 53:18–33. https://doi.org/10.1016/j.bbi.2015.08.010

42. Mizutani M, Pino PA, Saederup N, Charo IF, Ransohoff RM, Cardona AE (2012) The fractalkine receptor but not CCR2 is present on microglia from embryonic development throughout adulthood. J Immunol 188:29–36. https://doi.org/10.4049/jimmunol.1100421

43. Nakashima S (2002) Protein kinase C alpha (PKC alpha): regulation and biological function. J Biochem 132:669–675

44. Neuwelt EA, Garcia JH, Mena H (1978) Diffuse microglial proliferation after global ischemia in a patient with aplastic bone marrow. Acta Neuropathol 43:259–262

45. Newell EW, Schlichter LC (2005) Integration of K+ and Cl− currents regulate steady-state and dynamic membrane potentials in cultured rat microglia. J Physiol 567:869–890. https://doi.org/10.1113/jphysiol.2005.092056

46. Norenberg W, Gebicke-Haerter PJ, Illes P (1994) Voltage-dependent potassium channels in activated rat microglia. J Physiol 475:15–32

47. Norenberg W, Langosch JM, Gebicke-Haerter PJ, Illes P (1994) Characterization and possible function of adenosine 5′-triphosphate receptors in activated rat microglia. Br J Pharmacol 111:942–950

48. Pannasch U, Farber K, Nolte C, Blonski M, Yan Chiu S, Messing A, Kettenmann H (2006) The potassium channels Kv1.5 and Kv1.3 modulate distinct functions of microglia. Mol Cell Neurosci 33:401–411. https://doi.org/10.1016/j.mcn.2006.08.009

49. Panos M, Christophi GP, Rodriguez M, Scarisbrick IA (2014) Differential expression of multiple kallikreins in a viral model of multiple sclerosis points to unique roles in the innate and adaptive immune response. Biol Chem 395:1063–1073. https://doi.org/10.1515/hsz-2014-0141

50. Paolicelli RC, Bolasco G, Pagani F, Maggi L, Scianni M, Panzanelli P, Giustetto M, Ferreira TA, Guiducci E, Dumas L et al (2011) Synaptic pruning by microglia is necessary for normal brain development. Science 333:1456–1458. https://doi.org/10.1126/science.1202529

51. Peri F, Nusslein-Volhard C (2008) Live imaging of neuronal degradation by microglia reveals a role for v0-ATPase a1 in phagosomal fusion in vivo. Cell 133:916–927. https://doi.org/10.1016/j.cell.2008.04.037

52. Perry VH, Andersson PB, Gordon S (1993) Macrophages and inflammation in the central nervous system. Trends Neurosci 16:268–273

53. Phillips JW, Barringhaus KG, Sanders JM, Hesselbacher SE, Czarnik AC, Manka D, Vestweber D, Ley K, Sarembock IJ (2003) Single injection of P-selectin or P-selectin glycoprotein ligand-1 monoclonal antibody blocks neointima formation after arterial injury in apolipoprotein E-deficient mice. Circulation 107:2244–2249. https://doi.org/10.1161/01.CIR.0000065604.56839.18

54. Planas AM, Gorina R, Chamorro A (2006) Signalling pathways mediating inflammatory responses in brain ischaemia. Biochem Soc Trans 34:1267–1270. https://doi.org/10.1042/BST0341267

55. Priller J, Flugel A, Wehner T, Boentert M, Haas CA, Prinz M, Fernandez-Klett F, Prass K, Bechmann I, de Boer BA et al (2001) Targeting gene-modified hematopoietic cells to the central nervous system: use of green fluorescent protein uncovers microglial engraftment. Nat Med 7:1356–1361. https://doi.org/10.1038/nm1201-1356

56. Prinz M, Priller J (2017) The role of peripheral immune cells in the CNS in steady state and disease. Nat Neurosci 20:136–144. https://doi.org/10.1038/nn.4475

57. Ramos-Sevillano E, Urzainqui A, de Andres B, Gonzalez-Tajuelo R, Domenech M, Gonzalez-Camacho F, Sanchez-Madrid F, Brown JS, Garcia E, Yuste J (2016) PSGL-1 on leukocytes is a critical component of the host immune response against invasive pneumococcal disease. PLoS Pathog 12:e1005500. https://doi.org/10.1371/journal.ppat.1005500

58. Ransohoff RM, Stevens B (2011) Neuroscience. How many cell types does it take to wire a brain? Science 333:1391–1392. https://doi.org/10.1126/science.1212112

59. Ritzel RM, Patel AR, Grenier JM, Crapser J, Verma R, Jellison ER, McCullough LD (2015) Functional differences between microglia and monocytes after ischemic stroke. J Neuroinflammation 12:106. https://doi.org/10.1186/s12974-015-0329-1

60. Sako D, Comess KM, Barone KM, Camphausen RT, Cumming DA, Shaw GD (1995) A sulfated peptide segment at the amino terminus of PSGL-1 is critical for P-selectin binding. Cell 83:323–331

61. Sasmono RT, Oceandy D, Pollard JW, Tong W, Pavli P, Wainwright BJ, Ostrowski MC, Himes SR, Hume DA (2003) A macrophage colony-stimulating factor receptor-green fluorescent protein transgene is expressed throughout the mononuclear phagocyte system of the mouse. Blood 101:1155–1163. https://doi.org/10.1182/blood-2002-02-0569

62. Sasmono RT, Williams E (2012) Generation and characterization of MacGreen mice, the Cfs1r-EGFP transgenic mice. Methods Mol Biol 844:157–176. https://doi.org/10.1007/978-1-61779-527-5_11

63. Schall TJ, Proudfoot AE (2011) Overcoming hurdles in developing successful drugs targeting chemokine receptors. Nat Rev Immunol 11:355–363. https://doi.org/10.1038/nri2972

64. Schulz C, Gomez Perdiguero E, Chorro L, Szabo-Rogers H, Cagnard N, Kierdorf K, Prinz M, Wu B, Jacobsen SE, Pollard JW et al (2012) A lineage of myeloid cells independent of Myb and hematopoietic stem cells. Science 336:86–90. https://doi.org/10.1126/science.1219179

65. Spertini C, Baisse B, Spertini O (2012) Ezrin-radixin-moesin-binding sequence of PSGL-1 glycoprotein regulates leukocyte rolling on selectins and activation of extracellular signal-regulated kinases. J Biol Chem 287:10693–10702. https://doi.org/10.1074/jbc.M111.318022

66. Spertini O, Cordey AS, Monai N, Giuffre L, Schapira M (1996) P-selectin glycoprotein ligand 1 is a ligand for L-selectin on neutrophils, monocytes, and CD34+ hematopoietic progenitor cells. J Cell Biol 135:523–531

67. Starck L, Popp K, Pircher H, Uckert W (2014) Immunotherapy with TCR-redirected T cells: comparison of TCR-transduced and TCR-engineered hematopoietic stem cell-derived T cells. J Immunol 192:206–213. https://doi.org/10.4049/jimmunol.1202591

68. Swiatkowski P, Murugan M, Eyo UB, Wang Y, Rangaraju S, Oh SB, Wu LJ (2016) Activation of microglial P2Y12 receptor is required for outward potassium currents in response to neuronal injury. Neuroscience 318:22–33. https://doi.org/10.1016/j.neuroscience.2016.01.008

69. Szekanecz Z, Koch AE (2016) Successes and failures of chemokine-pathway targeting in rheumatoid arthritis. Nat Rev Rheumatol 12:5–13. https://doi.org/10.1038/nrrheum.2015.157

70. Tanaka R, Komine-Kobayashi M, Mochizuki H, Yamada M, Furuya T, Migita M, Shimada T, Mizuno Y, Urabe T (2003) Migration of enhanced green fluorescent protein expressing bone marrow-derived microglia/macrophage into the mouse brain following permanent focal ischemia. Neuroscience 117:531–539

71. Ullrich N, Strecker JK, Minnerup J, Schilling M (2014) The temporo-spatial localization of polymorphonuclear cells related to the neurovascular unit after transient focal cerebral ischemia. Brain Res 1586:184–192. https://doi.org/10.1016/j.brainres.2014.08.037

72. Villa E, Critelli R, Lei B, Marzocchi G, Camma C, Giannelli G, Pontisso P, Cabibbo G, Enea M, Colopi S et al (2016) Neoangiogenesis-related genes are hallmarks of fast-growing hepatocellular carcinomas and worst survival. Results from a prospective study. Gut 65:861–869. https://doi.org/10.1136/gutjnl-2014-308483

73. Visentin S, Renzi M, Levi G (2001) Altered outward-rectifying K(+) current reveals microglial activation induced by HIV-1 Tat protein. Glia 33:181–190

74. Walzlein JH, Synowitz M, Engels B, Markovic DS, Gabrusiewicz K, Nikolaev E, Yoshikawa K, Kaminska B, Kempermann G, Uckert W et al (2008) The antitumorigenic response of neural precursors depends on subventricular proliferation and age. Stem cells 26:2945–2954. https://doi.org/10.1634/stemcells.2008-0307

75. Wattananit S, Tornero D, Graubardt N, Memanishvili T, Monni E, Tatarishvili J, Miskinyte G, Ge R, Ahlenius H, Lindvall O et al (2016) Monocyte-derived macrophages contribute to spontaneous long-term functional recovery after stroke in mice. J Neurosci 36:4182–4195. https://doi.org/10.1523/JNEUROSCI.4317-15.2016

76. Weng L, Dai H, Zhan Y, He Y, Stepaniants SB, Bassett DE (2006) Rosetta error model for gene expression analysis. Bioinformatics 22:1111–1121. https://doi.org/10.1093/bioinformatics/btl045

77. Wirenfeldt M, Dissing-Olesen L, Anne Babcock A, Nielsen M, Meldgaard M, Zimmer J, Azcoitia I, Leslie RG, Dagnaes-Hansen F, Finsen B (2007) Population control of resident and immigrant microglia by mitosis and apoptosis. Am J Pathol 171:617–631. https://doi.org/10.2353/ajpath.2007.061044

78. Xia L, Sperandio M, Yago T, McDaniel JM, Cummings RD, Pearson-White S, Ley K, McEver RP (2002) P-selectin glycoprotein ligand-1-deficient mice have impaired leukocyte tethering to E-selectin under flow. J Clin Investig 109:939–950. https://doi.org/10.1172/JCI14151

79. Yamasaki R, Lu H, Butovsky O, Ohno N, Rietsch AM, Cialic R, Wu PM, Doykan CE, Lin J, Cotleur AC et al (2014) Differential roles of microglia and monocytes in the inflamed central nervous system. J Exp Med 211:1533–1549. https://doi.org/10.1084/jem.20132477

80. Yildirim F, Ji S, Kronenberg G, Barco A, Olivares R, Benito E, Dirnagl U, Gertz K, Endres M, Harms C et al (2014) Histone acetylation and CREB binding protein are required for neuronal resistance against ischemic injury. PLoS One 9:e95465. https://doi.org/10.1371/journal.pone.0095465

81. Zhou J, Neale JH, Pomper MG, Kozikowski AP (2005) NAAG peptidase inhibitors and their potential for diagnosis and therapy. Nat Rev Drug Discov 4:1015–1026. https://doi.org/10.1038/nrd1903